Modelling of photo-electrocatalytic behaviour of TiO_2 nanotubes under solar light irradiation

Laura Mais, Michele Mascia*, Simonetta Palmas, Annalisa Vacca

Università degli studi di Cagliari, Dipartimento di Ingegneria Meccanica, Chimica e dei Materiali, via Marengo 2, 09123, Cagliari (Italy)

*corresponding author: michele.mascia@unica.it, +39 0706755054

Abstract

A mathematical model of the photo-electrochemical processes occurring during irradiation with solar light has been implemented, to evaluate the optimal geometry of TiO_2 nanotubular structures for the different applications. The model accounts for generation and recombination of charge carriers, as well as for transport phenomena in solid phase. Electrochemical reactions at the surface and chemical processes in liquid phase are also modelled. The solar irradiation has been discretised in the UV and visible range, and adsorption coefficients as a function of the wavelength have been used. The model has been solved for oxidation of water, as well as for oxidation of organic compounds with different reactivity. The effect of such variables as light intensity, electric potential and reactivity of the organic compounds on space distribution of charge carriers in solid phase, oxygenated radicals and organic compounds in liquid phase, have been determined. The model provides a versatile tool to assess the performances of nanotubular electrodes at microscale and makes possible the optimal design of the nanostructure.

Keywords: Modelling, Photo-electrocatalysis, TiO_2 nanotubes, Oxidation of Organics

List of Symbols

Symbol	Description	[unit]
c	Speed of light	2.99×10^{8} [m/s]
C_i	Concentration of the i^{th} compound	[mol m^{-3}]
d	Tube diameter	[nm]
D_i	Diffusion of the i^{th} specie	[m^2 s^{-1}]
e	Electron charge	1.6×10^{-19} [C]
F	Faraday's constant	96500[C mol^{-1}]
h	Planck's constant	6.63×10^{-34} [Js]
I_0	Light intensity	[W m^{-2}]
k_B	Boltzmann constant	1.38×10^{-23} [JK^{-1}]
k_i	Specific reaction rate	[m^3 mol^{-1} s^{-1}]
K^L_{Org}	Isotherm parameter	[m^3*mol^{-1}]
k_R	Recombination rate	[s^{-1}]
L	Length of nanotubes	[µm]
N_D	Charge density TiO_2	[cm^{-3}]
y	Distance from the surface	[nm]
α	Specific absorption coefficient	[m^{-1}]
δ	Wall thickness	[nm]
θ_{MAX}	Surface density of active sites	[mol cm^{-2}]
μ	Mobility of species	[m^2 V^{-1} s^{-1}]
z	Charge of species	
λ	Wavelength	[nm]
ϕ	Electric Potential	[V]
Φ_2	Thiele modulus	
ζ	Lumped parameter in eq.12	
η	Anode overpotential	[V]
ε_0	Electric constant	8.85×10^{-12}[F/m]
ε_{TiO2}	Dielectric constant TiO_2	114

Acronym	Description
cc	Charge carriers
ox	Oxygenated radicals
org	Organic compounds

Introduction

Nowadays, the use of porous electrodes, with high specific surface area, has become almost mandatory to obtain highly performing devices in both electro- and photo-electrocatalytic processes [1]: at fixed potential, highly porous structures may provide electrical current at least one order of magnitude higher than that of flat electrodes with the same geometric area, thus making possible a reduction of the overall macroscopic size of the related device.

In addition to the specific surface area, other factors may influence electrode performances, such as the dimensions of pores and their aspect ratio (length / diameter, L/D), as well as the characteristics of the solute (molecular size, diffusivity and reactivity) [2, 3]. The list is even longer, when also the effect of the light is involved, as in photo-electrocatalytic processes: in this case, also the light absorption ability of the material, the transfer rate of photogenerated charges and their recombination rate inside the porous matrix, are important factors in determining the whole performance of the electrode [4, 5].

Among the electrode materials used for applications in photo-electrocatalytic processes, such as water splitting for H_2 production or organic oxidation, nanotubular structures (NT) of TiO_2 received a great attention [6-9]. Their architecture, consisting of vertically oriented, highly ordered nanotubes, allows high surface area-to-volume ratio [10], and enhances electron transport velocity and charge separation efficiency, reducing charge recombination rate, so making these materials ideal for photo-electrocatalytic applications [11, 12].

Great attention has been paid on the development of suitable techniques to build-up this kind of structures, and to investigate on possible parameters which may be effective on their performances. When NT are used in organic photo-electro-degradation processes, diffusion of compounds within the pores and adsorption on the surface of TiO_2 may

influence the process and, in some cases, affect the related organic degradation efficiency. With high concentrated solutions, adsorption of organics may decrease the availability of the active sites for the generation of hydroxyl radicals; furthermore, the photons could be intercepted before they could reach the catalyst surface, reducing the degradation efficiency [13].

In addition to the concentration, the effective exploitation of the surface area is worth to be considered, in terms of surface available for both oxidation and photoelectric effect. The tube morphology should allow the entire UV light to be absorbed, without limiting the reactant diffusion inside pores.

Previous studies demonstrated the key role of the morphological factor on the photocatalytic activity of TiO_2. Pasikhani et al. showed that the increase in the length-to-diameter (L/D) ratio of the TiO_2 nanotubes resulted in greater light absorption, leading to an increase in photocurrent density and photoconversion efficiency, thanks to the decrease in the electron/hole pairs recombination and to the increase in the active site density for photocatalytic degradation [14]. Several works report the effect of tube lengths on the performance of photocatalytic degradation: depending on the wavelengths adopted in the experiments, high values ranging from 6 to 18 μm have been reported as optimal [15-19], even if the UV light is only absorbed in the first 1-2 μm [20]. Depending on the synthesis conditions used in the anodization process, D and L of the tubes are often found to be correlated [21].

The above considerations shed light on the importance of the engineering of the nanotubular structure, as the question on how to individuate the pore architectures to maximise the performance of the structure for a given process, is still open.

In this work we aim to contribute filling this gap, using mathematical model to predict the effect of both organic compounds and light absorption on different NT morphologies and under different operative conditions. The model considers phenomena in the solid phase, such as formation and recombination of electron-hole pairs, and chemical and electrochemical reactions in the liquid phase. Transport of species in liquid and solid phase are also accounted for. The model solution gives 2D profiles of charge carriers and chemical species for different lengths of NT and thickness of pore wall. It makes possible a systematic investigation on the effect of operative parameters, as well as an accurate evaluation of the optimal geometry of the nanotubular structure for the different applications. To the best of our knowledge few attempts were made to implement multi-dimensional models of the porous systems in which diffusion and electrochemical reactions are accounted for [1, 22, 23]. The novelty of the paper rests on the 2D modelling in which chemical and electrochemical phenomena within nanotube volume, are combined with photochemical processes in solid phase; moreover, the model accounts for light absorption and photoelectrochemical processes in the whole wavelength of the solar spectrum, while previous papers mainly focused on single wavelength value.

1. Model description

As the morphology of TiO_2 nanotubes is concerned, they usually show quasi-circular base and different diameters, although in a narrow range of values. Tubes usually feature with rough inner surface and hemi-spherical bottom [24,25]. For the sake of modelling, the nanotubes are represented as cylinders, and the activity of the bottom surface, which amounts to some percentile of the whole surface, was not considered. However, in the parametrisation of the model, active surface and transport properties of real nanotubes were used, so that the model assumption is of cylindrical pores equivalent to real pores.

Following the mechanism widely adopted in the literature, TiO_2 photocatalytic processes involve solid–state surface redox transitions as well as adsorption steps; the oxidation of organics mainly proceeds by oxygenated radicals such as $OH^{\bullet}$, produced by reaction of photoinduced holes (charge carriers) with hydroxide ions or water molecules [26-28].

The mechanisms involved in aqueous media at TiO_2 starts from the formation of electron/hole pairs:

(1)

The oxidation of water molecules by photogenerated positive holes forms hydroxyl radicals which can react with the organic compounds, leading to oxidised species and/or decomposed product:

(2)

(3)

Also adsorbed oxygen can react with electron to form super oxide ions which can be able to oxidise the pollutants:

(4)

(5)

The direct reaction of the photogenerated holes with organic compounds at the TiO_2 surface [29] is another possible process [14]:

(6)

However, the reaction of oxygenated radicals with organics is much faster than the oxidation, by direct electron transfer, of organics adsorbed on the TiO_2 surface [30]. Direct oxidation was then neglected, and the whole surface of TiO_2, free of organic coverage, was considered available for radical generation [31].

Adsorption of organics at the TiO_2 surface has been described with a potential-dependent Langmuir isotherm [32,33].

(7)

The generation rate of charge carriers depends on the distance from the surface of the nanotubular layer, through a Lambert-Beer dependence: a literature value of 500 m^{-1} for the absorption coefficient was used [34,35].

The recombination rate follows a pseudo-first order kinetics, and the specific reaction rate depends on the recombination time, with a value of 2 x 10^{10} s^{-1} [35-37]. At the surface/electrolyte interface, the charge carriers react with water to give oxygenated radicals, with a potential dependent kinetics.

Finally, a second order kinetics is assumed for the reaction rates of organics with radicals.

The system was then modelled as combination of quasi-homogeneous media, with three integration domains:

1) solid phase: which includes walls and bottom of the pores;

2) liquid phase: liquid volume within the pores;

3) diffusion layer: liquid outside of pores.

Figure 1 shows a sketch of geometry and domains of integration. The model equations were written for each domain.

Figure 1

In the solid-phase domain, the concentration of charge carriers (CC) generated by incident photons was represented by a transport equation in homogeneous medium, which accounts for diffusion, migration and reactions of generation and recombination.

(8)

R_{CC} is the reaction term:

(9)

where the first and second terms on the right side correspond to the rate of photo generation of holes, and to the pseudo-first order rate of recombination, respectively.

The generation of charge carriers was modelled with discrete intervals *i* of wavelengths of 50 nm:

(10)

α and I_0 are functions of the wavelength λ. Data of absorption values, measured at different wavelengths for TiO_2 nanotube, were derived from literature [35,38], and interpolated with the following:

(11)

The overall light intensity of the solar spectrum I_0 can be calculated as ζB_λ, where B_λ is expressed by the Planck's law and ζ is a lumped parameter which accounts for different irradiation conditions:

(12)

To obtain the value of ζ, equation 12 was integrated in the whole range of the solar irradiation, and ζ was adjusted to fit the values of global radiation of the reference AM1.5 spectra [39].

Equation 12 was then used to calculate the values of I_{0i} in equation 10.

The migration term (the second one, in the right side of equation 1), is governed by the electric potential, which satisfies the Poisson's equation, in which the literature value of 10^{16} cm^{-3} was used for N_D [40,41]

(13)

In the liquid-phase and diffusion layer domains, the concentrations of organic (C_{Org}) compounds and oxygenated radicals (C_{OH}) generated at the electrode/electrolyte interfaces, were represented by the following diffusion/reaction equations:

(14)

(15)

with the corresponding reaction rate equations

(16)

(17)

Boundary conditions at the nanotube surfaces were: equal flux of charge carriers and oxygenated radicals (eq. 18), and null flux of organics (eq. 20):

(18)

(19)

The flux of organics at the same interface is null

(20)

At the diffusion boundary layer, the concentration of organics is a function of time

(21)

The numerical model was implemented and solved with the COMSOL Multiphysics® software.

Although the internal area of nanotubes with 1.5 μm length is considered as effective for generation of oxygenated radicals, when the photoelectrochemical process is addressed

to remove organic compounds from water, diffusion and reactivity will determine the optimal length [21]. In order to test the model, we have selected three different organic compounds, characterised by different reactivity with oxygenated radicals, and different diffusion coefficients: the first, phenol, is largely used as model substance in photoelectrochemical systems, and it is well known for the high reactivity with oxygenated radicals [42-44]; the second, oxalic acid, also typically tested in different AOPs, such as photoelectrochemical processes [45], is among the less reactive organic compounds investigated in the literature [46]; the third is the pesticide paraquat, which shows intermediate properties between phenol and oxalic acid [21].

To summarise the effect of the two parameters (diffusion coefficient and kinetic constant), the Thiele modulus has been used, which gives a rough evaluation of the catalytic behaviour of a porous catalyst. For the system considered, with second order kinetics reactions, the Thiele modulus can be written as:

(22)

In our system, the concentration of oxygenated radicals is not a constant, but we can calculate a relative Thiele modulus, using the most reactive compound as reference. The results are summarised in table 1.

Table 1: Diffusion coefficient, kinetic constant and relative Thiele modulus for the different organic compounds

	$10^9 x D_{org}$ **[$m^2 s^{-1}$]**	***k*** **[$m^3 mol^{-1} s^{-1}$]**	**Relative ϕ_2**
Phenol	3.76	6.20×10^9	1.0000
Oxalic acid	6.21	6.50×10^8	0.0634
Paraquat	3.68	1.00×10^7	0.0016

Specific reaction rates of organics with oxygenated radicals, were derived from literature [47]. Diffusion coefficients in the diffusion layer were calculated with the correlation of Wilke and Chang [48]. Since the values in Table 1 are very different, the selected compounds can be representative of a wide class of organics.

In the model solution, the diffusion of organic compounds in water accounts for possible effects of roughness of walls and nano-size of the pores. According to the literature, the diffusion within pores with diameter of some tens of nanometres follows the classical Fick's law [49,50]: the diffusion coefficients were adjusted according to the results obtained from measures of transport of species throughout TiO_2 nanotubular membranes [51,52]. According to Paulose et al, a linear function of the molecular weight was used as correction coefficient [51,53]. The surface concentration of active sites (0.98×10^{-7} mol cm^{-2}) was evaluated in previous work [30]. The value of self-diffusion coefficient of water was used for oxygenated radicals in equation 15 [54].

2. Results and discussion

Figure 2 shows an example of profiles of oxygenated radicals (C_{ox}) in liquid phase and charge carriers (C_{cc}) in solid phase, calculated with the model, under different operative conditions.

Figure 2

As it can be observed, the profiles calculated with the model do not show appreciable variations at a distance from the surface higher than few microns, so that in next figures the top of the pores (down to 1.5 μm) and the layer adjacent to the electrode surface are shown, where the most relevant phenomena occur. From the model predictions shown in figures 3, 4 and 5, the effect of different parameters can be observed.

Figure 3.

Figure 4.

Figure 5.

The generation of oxygenated radicals is influenced by the thickness of the pore wall: higher concentrations are obtained with higher pore thickness, which was also observed in the literature and attributed to the large amount of photogenerated electron/hole pairs [55], which is correctly predicted by the model. As the space distribution of oxidants is concerned, the literature reports occurrence of concentration gradients in liquid phase, due to the high reactivity of oxygenated radicals [54,56]: the model well interprets this behaviour, with two-dimensional concentration gradients, mainly located near the pore mouth. A noticeable feature is the difference between pore volume and diffusion layer: in

the region adjacent to the electrode surface the model predictions show strong decrease of concentration of radicals, as it was obtained with simulations in previous papers [54].

The diameter of the pore is relevant for the local concentration of oxygenated radicals: in the literature, mathematical models predict space profile these radicals where the concentration sharply decrease with the distance from the electrode surface. Oxygenated radicals show concentration values effective for reactions with organics in a layer of few tens of nanometres [57]. The morphology of nanotubes depends on such anodization conditions as applied potential and composition of the electrolyte [58]; however, diameters in the order of tens nanometres are usually obtained. This, along with the quasi-axial symmetry of the tubes makes possible relatively high concentration in the whole volume of the pores.

The effect of the applied potential can be also observed: the concentration of charge carriers decreases as the applied potential increases, due to the higher driving force for the electron transfer to the counter electrode, as well as the consumption of charge carriers by generation of oxygenated radicals, which in turn enhance the separation of the photo-generated electron/holes pairs [59].

A key parameter for the process is the light intensity: the model well predicts the increase of charge carriers and oxygenated radicals' concentration with the intensity of incident light, due to the higher probability of excitation and re-excitation of recombined electrons [60].

As the electrical current is concerned, figure 6 shows the ratio between current intensities, calculated under different conditions, and the maximum value of current intensity obtained with I_0 = 1000 Wm^{-2}, L=15 μm and δ = 40 nm.

Figure 6:

A linear dependence of current with light intensity is obtained, as it was also experimentally observed [31]. The current intensity increases with tube length (L) and wall thickness (δ), although the corresponding densities (not showed) decrease as L increases. The effect of wall thickness depends on the number of electron/hole pairs, as already observed. The effect of pore length may be due to the large surface area available for reaction of charge carriers with the electrolyte; this can be still exploited with pores of 1.5 μm length, where wavelengths of near visible UV can penetrate [51].

To evaluate the effects of geometry of the pores, operative conditions and properties of the compounds during oxidation of organics under different operative conditions, simulations were carried out with several input parameters. Although the model equations can predict 2D profiles, from the solutions we can only observe concentration gradients of organics in the direction of the pore axis, whereas the concentration is nearly constant in the direction perpendicular to the pore axis. This is due to the small pore diameters and to the relatively high values of diffusion coefficients of most of organic compounds in water; in the following figures, the results are then presented as profiles of organics with the pore length.

Photo electrochemical oxidation of phenol (A), paraquat (B) and oxalic acid (C) was simulated with L = 10 μm, d = 100 nm, δ = 40 nm, I_0 = 1000 W m^{-2} and η = 1V. The profiles of concentration along the pores, calculated with the model are depicted in Figure 7.

The results of the model predictions show that with low concentration of organic in the solution, the whole surface of the tubes is effective only for oxidation of the less reactive compound: as the reactivity with oxygenated radicals increases, the effective surface decreases. Moreover, appreciable differences between phenol and paraquat can be observed only with the lowest concentration. If purification of water is the aim of the process, tubes with 4 μm length or less should be used for compounds with reactivity like

paraquat, while 2 μm is effective for removal of very reactive compounds, such as phenol. Longer tubes should be considered for wastewater treatment, with high pollutant concentrations. Nanotubular TiO_2 electrodes with thickness in the order of ten micrometres were found to be effective for such applications [21].

Figure 7.

Figure 8 shows the effect of light intensity and bias potential on the concentration profiles inside the pores, with 0.5 mol m^{-3} of bulk concentration.

Figure 8.

With reactive compounds, low intensities of radiation make possible to exploit most of the pore surface, when low bias potentials are used, while the effective surface decreases as potential and radiation increase. Oxidation of compounds with low reactivity shows an effective area corresponding to the whole length of tubes under all the conditions simulated.

The effect of tube geometry is shown in figure 9, where the results of simulations with different pore length and wall thickness are depicted.

Figure 9.

With I_0 = 1000 W m^{-2} and reactive compounds, the maximum decrease in concentration along the pores is reached with L = 10 μm and δ = 40 nm, or L = 15 μm and δ = 20 nm. When the oxidation of phenol and paraquat is considered, about half the surface is effective, due to the high oxidising conditions inside the pores. To exploit the whole pore length, lower light intensities should be used.

Figure 10.

Figure 10 shows the effect of the presence of organic compounds on the concentration of oxygenated radicals within the pores and in the diffusion layer. Results calculated with

paraquat and oxalic acid and different light intensities are reported. The reactivity of organics influences the concentration of radicals; the model well predicts the different scavenger effect of compounds with high and low reactivity.

Conclusions

A mathematical model was implemented and solved to represent photochemical, chemical and electrochemical processes, and transport phenomena which occur during photo electrochemical oxidation of organic compounds with TiO_2 nanotubular electrodes.

The effect of such variables as light intensity, electric potential and organic reactivity, were quantified.

The key parameters of the process were light intensity, potential and reactivity of organics with oxygenated radicals generated by water oxidation at the electrode surface. Depending on reactivity and concentration of the compounds, the optimal length of nanotubes is different: tubes of 10 μm length are effective with high concentrations, while shorter tubes can be used where low-concentrated organic compounds must be removed.

The model provides a versatile tool to assess the performances of nanotubular electrodes at microscale and makes possible the optimal design of the nanostructure.

Based on the results of the model, tubes with high length and wall thickness should be used to maximise the current generation, although the feasibility of such structures should be verified. The geometry of the pores is constrained; as reported in literature, the lengths depend on the anodization potential [62]; however, the dissolution of the nanotube wall limits the achievable nanotube length and prevents to achieve higher aspect ratio tubes for example by extended anodization [63] .

The model predicts the performances of the electrode at nanoscale and is the first step in developing design tool for TiO_2-based photoelectrochemical reactors. The model

parameters are based on literature data, however, a direct comparison of the predictions with experimental data is not straightforward, due to the scale of the phenomena considered. This work will be followed by a 3D model of the whole electrode, with geometrical optimisation of nanotubular photo-anodes, and comparison of model predictions with experimental data. This will make it possible design of solar photoelectrochemical processes for such application as hydrogen generation, water treatment and disinfection.

Acknowledgements

Funding: This work was supported by Fondazione di Sardegna, Project NAMEFOAMS, F72F16003180002, F71I17000280002-2017.

References

[1] T.D. Le, D. Lasseux, X.P. Nguyen, G. Vignoles, N. Mano, A. Kuhn, Multi-scale modeling of diffusion and electrochemical reactions in porous micro-electrodes, Chem. Eng. Sci. 173 (2017) 153–167. https://doi.org/10.1016/j.ces.2017.07.039.

[2] C. Adán, J. Marugán, E. Sánchez, C. Pablos, R. van Grieken, Understanding the effect of morphology on the photocatalytic activity of TiO_2 nanotube array electrodes, Electrochim. Acta 191 (2016) 521–529. https://doi.org/10.1016/j.electacta.2016.01.088.

[3] L. Mais, S. Palmas, M. Mascia, E. Sechi, M.F. Casula, J. Rodriguez, A. Vacca, Porous Ni photocathodes obtained by selective corrosion of Ni-Cu films: Synthesis and photoelectrochemical characterization, Catalysts 9 (2019) 453. https://doi.org/10.3390/catal9050453.

[4] V. Likodimos, T. Stergiopoulos, P. Falaras, J. Kunze, P. Schmuki, Phase composition, size, orientation, and antenna effects of self-assembled anodized titania nanotube arrays: A polarized micro-Raman investigation, J. Phys. Chem. C 112 (2008) 12687–12696. https://doi.org/10.1021/jp8027462.

[5] Y. Alivov, M. Pandikunta, S. Nikishin, Z.Y. Fan, The anodization voltage influence on the properties of TiO_2 nanotubes grown by electrochemical oxidation, Nanotechnology 20 (2009) 225602–225608. https://doi.org/10.1088/0957-4484/20/22/225602.

[6] Y. Fu, A. Mo, A review on the electrochemically self-organized titania nanotube arrays: synthesis, modifications, and biomedical applications, Nanoscale Res Lett. 13 (2018) 187-208. https://doi.org/10.1186/s11671-018-2597-z.

[7] S. Shen, J. Chen, M. Wang, X. Sheng, X. Chen, X. Feng, S. S. Mao, Titanium dioxide nanostructures for photoelectrochemical applications, Prog. Mater Sci. 98 (2018) 299-385. https://doi.org/10.1016/j.pmatsci.2018.07.006.

[8] S. Palmas, M. Mascia, A. Vacca, J. Llanos, E. Mena, Analysis of photocurrent and capacitance of TiO_2 nanotube-polyaniline hybrid composites synthesized through electroreduction of an aryldiazonium salt, RSC Advances 4 (2014) 24957-24965. https://doi.org/10.1039/C4RA01712A.

[9] S. Palmas, A. Da Pozzo, M. Mascia, A. Vacca, P.C. Ricci, Sensitization of TiO_2 nanostructures with Coumarin 343, Chem. Eng. J. 211-212 (2012) 285-292. https://doi.org/10.1016/j.cej.2012.09.093.

[10] H.C. Liang, X.Z. Li, Effects of structure of anodic TiO_2 nanotube arrays on photocatalytic activity for the degradation of 2,3-dichlorophenol in aqueous solution, J. Hazard. Mater. 162 (2008) 1415-1422. https://doi.org/10.1016/j.jhazmat.2008.06.033.

[11] S. Palmas, A. Da Pozzo, M. Mascia, A. Vacca, R. Matarrese, I. Nova. Photo-electrochemical behavior at different wavelengths of electrochemically obtained TiO_2 nanotubes, J. Appl. Electrochem. 42 (2012) 745–751. https://doi.org/10.1007/s10800-012-0456-7.

[12] S. Palmas, P.A. Castresana, L. Mais, A. Vacca, M. Mascia, P.C. Ricci, TiO_2-WO_3 nanostructured systems for photoelectrochemical applications, RSC Advances, 6 (2016) 101671-101682. https://doi.org/10.1039/C6RA18649A.

[13] N.A. Laoufi, D. Tassalit, F. Bentahar, The degradation of phenol in water solution by TiO_2 photocatalysis in a helical reactor, Global NEST J. 10 (2008) 404-418. https://doi.org/10.30955/gnj.000525.

[14] J. V. Pasikhani, N. Gilani, A. E. Pirbazari, Improvement the wastewater purification by TiO_2 nanotube arrays: the effect of etching-step on the photo-generated charge carriers and photocatalytic activity of anodic TiO_2 nanotubes, Solid State Sci. 84 (2018) 57-74. https://doi.org/10.1016/j.solidstatesciences.2018.08.003.

[15] Y.R. Smith, A. Kar, V. Subramanian, Investigation of physicochemical parameter that influence the photocatalytic degradation of methyl orange, Ind. Eng. Chem. Res. 48 (2009) 10268-10276. https://doi.org/10.1021/ie801851p.

[16] Z. Liu, X. Zhang, S. Nishimoto, M. Jin, D.A. Tryk, T. Murakami, A. Fujishima. Highly ordered TiO_2 nanotube arrays with controllable length for photoelectrocatalitic oxidation of phenol, J. Phys. Chem. C 112 (2008) 253-259. https://doi.org/10.1021/jp0772732.

[17] I. Paramasivam, H. Jha, N. Liu, P. Schmuki, A review of photocatalysis using self-organized TiO_2 nanotubes and other ordered oxide nanostructure, Small 8 (2012) 3073-3103. https://doi.org/10.1002/smll.201200564.

[18] A. Turki, C. Guillard, F. Dappozze, Z. Ksibi, G. Berhault, H. Kochkar, Phenol photocatalytic degradation over anisotropic TiO_2 nanomaterials, App. Cat. B: Environ. 163 (2015) 404-414. https://doi.org/10.1016/j.apcatb.2014.08.010.

[19] R. Mu, Z. Xu, L. Li, Y. Shao, H. Wan, S. Zheng, On the photocatalytic properties of elongated TiO_2 nanoparticles for phenol degradation and Cr(VI) reduction, J. Hazard. Mater. 176 (2010) 495-502. https://doi.org/10.1016/j.jhazmat.2009.11.057.

[20] C. Das, P. Roy, M. Yang, Himendra Jha and P. Schmuki Nb doped TiO_2 nanotubes for enhanced photoelectrochemical water-splitting, Nanoscale 3 (2011) 3094-3096. https://doi.org/10.1039/C1NR10539F.

[21] C.B.D. Marien, T. Cottineau, D. Robert, P. Drogui, TiO_2 Nanotube arrays: Influence of tube length on the photocatalytic degradation of Paraquat, Appl. Catal. B: Environ. 194 (2016) 1-6. https://doi.org/10.1016/j.apcatb.2016.04.040.

[22] T. D. Le, L. Zhang, S. Reculusa, G. Vignoles, N. Mano, A. Kuhn, D. Lasseux, Optimal Thickness of a Porous Micro-Electrode Operating a Single Redox Reaction, ChemElectroChem, 6 (2019) 173-180. https://doi.org/10.1002/celc.201800972.

[23] C. Ma, X. Li, L. Lin, L. Chen, M. Wang, J. Zhou, A two-dimensional porous electrode model for designing pore structure in a quinone-based flow cell, J. Energy Storage, 18 (2018) 16-25. https://doi.org/10.1016/j.est.2018.04.007.

[24] D. Kowalski, D. Kim, P. Schmuki, TiO_2 nanotubes, nanochannels and mesosponge: Self-organized formation and applications, Nano Today 8 (2013) 235–264. http://dx.doi.org/10.1016/j.nantod.2013.04.010.

[25] K. Lee, A. Mazare, P. Schmuki, One-Dimensional Titanium Dioxide Nanomaterials: Nanotubes, Chem. Rev. 114 (2014) 9385-9454. https://doi.org/10.1021/cr500061m.

[26] T. Hirakawa, K. Yawata, Y, Nosaka, Photocatalytic reactivity for O2•- and OH• radical formation in anatase and rutile TiO_2 suspension as the effect of H2O2 addition, Appl. Cat. A: Gen. 325 (2007) 105-111. https://doi.org/10.1016/j.apcata.2007.03.015.

[27] L. Sun, J.R. Bolton, Determination of the Quantum Yield for the Photochemical Generation of Hydroxyl Radicals in TiO_2 Suspensions, J. Phys. Chem. 100 (1996) 4127-4134. https://doi.org/10.1021/jp9505800.

[28] M.R. Hoffmann, S.T. Martin, W. Choi, D.W. Bahnemann, Environmental applications of semiconductor photocatalysis, Chem. Rev. 95 (1995) 69-96. https://doi.org/10.1021/cr00033a004.

[29] Y. Nosaka, S. Komori, K. Yawata, T. Hirakawa, A.Y. Nosaka, Photocatalytic OH radical formation in TiO_2 aqueous suspension studied by several detection methods, Phys. Chem. Chem. Phys. 5 (2003) 4731-4735. https://doi.org/10.1039/B307433A.

[30] C. Minero, G. Mariella, V. Maurino, and E. Pelizzetti, Photocatalytic transformation of organic compounds in the presence of inorganic anions. 1. hydroxyl-mediated and direct electron-transfer reactions of phenol on a titanium dioxide-fluoride system, Langmuir 16 (2000) 2632-2641. https://doi.org/10.1021/la9903301.

[31] L. Mais, M. Mascia, S. Palmas, A. Vacca, Photoelectrochemical oxidation of phenol with nanostructured TiO_2-PANI electrodes under solar light irradiation, Sep. Purif. Technol. 208 (2019) 153-159. https://doi.org/10.1016/j.seppur.2018.03.074.

[32] S. Palmas, F. Ferrara, M. Mascia, A. M. Polcaro, J. Rodriguez Ruiz, A. Vacca, G. Piccaluga, Modeling of oxygen evolution at Teflon-bonded Ti/Co_3O_4 electrodes, Int. J. Hydrogen Energy 34 (2009) 1647-1654. https://doi.org/10.1016/j.ijhydene.2008.11.104.

[33] S. Bekkouche, M. Bouhelassa, N.H. Salah, F.Z. Meghlaoui, Study of adsorption of phenol on titanium oxide (TiO_2), Desalination 166 (2004) 355-362. https://doi.org/ 10.1016/j.desal.2004.06.090.

[34] F.R. Cummings, L.J. Le Roux, M.K. Mathe, D. Knoesen, Structure induced optical properties of anodized TiO_2 nanotubes, Mater. Chem. Phys. 124 (2010) 234-242. https://doi.org/10.1016/j.matchemphys.2010.06.024.

[35] A.B. Walker, L.M. Peter, K. Lobato, P.J. Cameron, Analysis of Photovoltage Decay Transients in Dye-Sensitized Solar Cells, J. Phys. Chem. B 110 (2006) 25504-25507. https://doi.org/10.1021/jp064860z

[36] K. Ozawa, M. Emori, S. Yamamoto, R. Yukawa, S. Yamamoto, R. Hobara, K. Fujikawa, H. Sakama, I. Matsuda, Electron−Hole Recombination Time at TiO_2 Single-Crystal Surfaces: Influence of Surface Band Bending J. Phys. Chem. Lett. 5 (2014) 1953-1957. https://doi.org/10.1021/jz500770c.

[37] A.G. Agrios, P. Pichat, Recombination rate of photogenerated charges versus surface area: Opposing effects of TiO_2 sintering temperature on photocatalytic removal of phenol, anisole, and pyridine in water, J. Photochem. Photobiol., A 180 (2006) 130-135. https://doi.org/10.1016/j.jphotochem.2005.10.003.

[38] G. Cha, P. Schmuki, M. Altomare, Free-Standing Membranes to Study the Optical Properties of Anodic TiO_2 Nanotube Layers, Chem. Asian J. 11 (2016) 789-797. https://doi.org/10.1002/asia.201501336.

[39] US NREL, https://www.nrel.gov/grid/solar-resource/spectra-am1.5.html

[40] J. Ferber, J. Luther, Modeling of Photovoltage and Photocurrent in Dye-Sensitized Titanium Dioxide Solar Cells, J. Phys. Chem. B 105 (2001) 4895-4903. https://doi.org/10.1021/jp002928j.

[41] J.A.S. Ikeda, Y.M. Chiang, Space Charge Segregation at Grain Boundaries in Titanium Dioxide: I, Relationship between lattice Defect Chemistry and Space Charge Potential, J. Am. Ceram. Soc. 76 (1993) 2437-2446. https://doi.org/10.1111/j.1151-2916.1993.tb03964.x.

[42] D. Liu, Z. Zheng, C. Wang, Y. Yin, S. Liu, B. Yang, Z. Jiang, CdTe Quantum Dots Encapsulated ZnO Nanorods for Highly Efficient Photoelectrochemical Degradation of Phenols, J. Phys. Chem. C 117 (2013) 26529-26537. https://doi.org/10.1021/jp410692y.

[43] H. Park, A. Bak, Y.Y. Ahn, J. Choi, M.R. Hoffmann, Photoelectrochemical performance of multi-layered BiO_x–TiO_2/Ti electrodes for degradation of phenol and production of molecular hydrogen in water, J. Hazard. Mater. 211 (2012) 47-54. https://doi.org/10.1016/j.jhazmat.2011.05.009.

[44] D. Monllor-Satoca, R. Gómez, A photoelectrochemical and spectroscopic study of phenol and catechol oxidation on titanium dioxide nanoporous electrodes, Electrochim. Acta 55 (2010) 4661-4668. https://doi.org/10.1016/j.electacta.2010.03.045.

[45] G. Waldner, R. Gomez, M. Neumann-Spallart, Using photoelectrochemical measurements for distinguishing between direct and indirect hole transfer processes on anatase: Case of oxalic acid, Electrochim Acta 52 (2007) 2634-2639. https://doi.org/10.1016/j.electacta.2006.09.019.

[46] Y. Alsalka, A. Hakki, M. Fleisch, D.W. Bahnemann, Understanding the degradation pathways of oxalic acid in different photocatalytic systems: Towards simultaneous photocatalytic hydrogen evolution, J. Photochem. Photobiol. A 366 (2018) 81-90. https://doi.org/10.1016/j.jphotochem.2018.04.008.

[47] F. Ross and A.B. Ross, Selected Specific Rates of Reactions of Transient from Water in Aqueous Solution III Hydroxyl Radical and Perhydroxyl Radical and their Radical Ions, NSRDS-NBS59, US Dept. of Commerce, Washington, 1977.

[48] C. R. Wilke, P. Chang, Correlation of diffusion coefficients in dilute solutions, AlChE J. 1 (1955) 264-270. https://doi.org/10.1002/aic.690010222.

[49] A. Pimpinelli, M. Ferrari, A. Gratton, Scaling and crossovers in molecular transport in nano-fluidic systems, Appl. Phys. Lett. 103 (2013) 113104, https://doi.org/10.1063/1.4819156.

[50] W. Sparreboom, A. van den Berg, J.C.T. Eijkel, Principles and applications of nanofluidic transport, Nat. Nanotech. 4 (2009) 713, https://doi.org/10.1038/nnano.2009.332.

[51] M. Paulose, H.E. Prakasam, O.K. Varghese, L. Peng, K.C. Popat, G.K. Mor, T.A. Desai, C.A. Grimes, TiO_2 Nanotube Arrays of 1000 □m Length by Anodization of Titanium Foil: Phenol Red Diffusion, J. Phys. Chem. C 111 (2007) 14992, https://doi.org/10.1021/jp075258r.

[52] S.P. Albu, A. Ghicov, J.M. Macak, R. Hahn, P. Schmuki, Self-Organized, Free-Standing TiO_2 Nanotube Membrane for Flow-through Photocatalytic Applications, Nano Lett. 7 (2007) 1286, https://doi.org/10.1021/nl070264k.

[53] M. Paulose, L. Peng, K.C. Popat, O.K. Varghese, T.J. La Tempa, N. Bao, T.A. Desai, C.A. Grimes, Fabrication of mechanically robust, large area, polycrystalline nanotubular/porous TiO_2 membranes, J. Membr. Sci. 319 (2008) 199. http://dx.doi.org/10.1016/j.memsci.2008.03.050.

[54] M. Mascia, A. Vacca, S. Palmas, A.M. Polcaro, Kinetics of the electrochemical oxidation of organic compounds at BDD anodes: modelling of surface reactions, J. Appl. Electrochem. 37 (2007) 71. http://dx.doi.org/10.1007/s10800-006-9217-9.

[55] C.A. Grimes, Synthesis and application of highly ordered arrays of TiO_2 nanotubes, J. Mater. Chem. 17 (2007) 1451. https://doi.org/10.1039/B701168G.

[56] M.R. Hoffmann, S.T. Martin, W. Choi, D.W. Bahnemann, Environmental Applications of Semiconductor Photocatalysis, Chem. Rev. 95 (1995) 69. https://pubs.acs.org/doi/10.1021/cr00033a004.

[57] Z. Jie, Y. Nosaka, Mechanism of the OH Radical Generation in Photocatalysis with TiO_2 of Different Crystalline Types, J. Phys. Chem. C 118 (2014) 10824-10832. https://doi.org/10.1021/jp501214m.

[58] F. Yang, X. Feng, F. Ge, T. Zhang, J. Qi, D. Li, X. Zhu, Rapid growth of titanium oxide nanotubes under the critical breakdown voltage: Evidence against the dissolution reaction

of fluoride ions, Electrochem. Commun. 103 (2019) 17-21. https://doi.org/10.1016/j.elecom.2019.04.010.

[59] N. Wang, X. Li, Y. Wang, X. Quan, G. Chen, Evaluation of bias potential enhanced photocatalytic degradation of 4-chlorophenol with TiO_2 nanotube fabricated by anodic oxidation method, Chem. Eng. J. 146 (2009) 30-35. http://dx.doi.org/10.1016/j.cej.2008.05.025.

[60] M.Z. Wang, F.X. Liang, B. Nie, L.H. Zeng, L.X. Zheng, P. Lv, Y.Q. Yu, C. Xie, Y.Y. Li, L.B. Luo, TiO_2 Nanotube Array/Monolayer Graphene Film Schottky Junction Ultraviolet Light Photodetectors, Part. Part. Syst. Charact. 30 (2013) 630. https://doi.org/10.1002/ppsc.201300040.

[61] R. Beranek, J.M. Macak, M. Gärtner, K. Meyer, P. Schmuki, Enhanced visible light photocurrent generation at surface-modified TiO_2 nanotubes, Electrochim. Acta 54 (2009) 2640. http://dx.doi.org/10.1016/j.electacta.2008.10.063.

[62] J.M.Macak, H. Hildebrand, U. Marten-Jahns, P.Schmuki, Mechanistic aspects and growth of large diameter self-organized TiO_2 nanotubes, J. Electroanal. Chem. 621 (2008) 254. http://dx.doi.org/10.1016/j.jelechem.2008.01.005.

[63] K. Yasuda, P. Schmuki, Control of morphology and composition of self-organized zirconium titanate nanotubes formed in $(NH_4)2SO_4/NH_4F$ electrolytes, Electrochim. Acta 52 (2007) 4053. http://dx.doi.org/10.1016/j.electacta.2006.11.023.

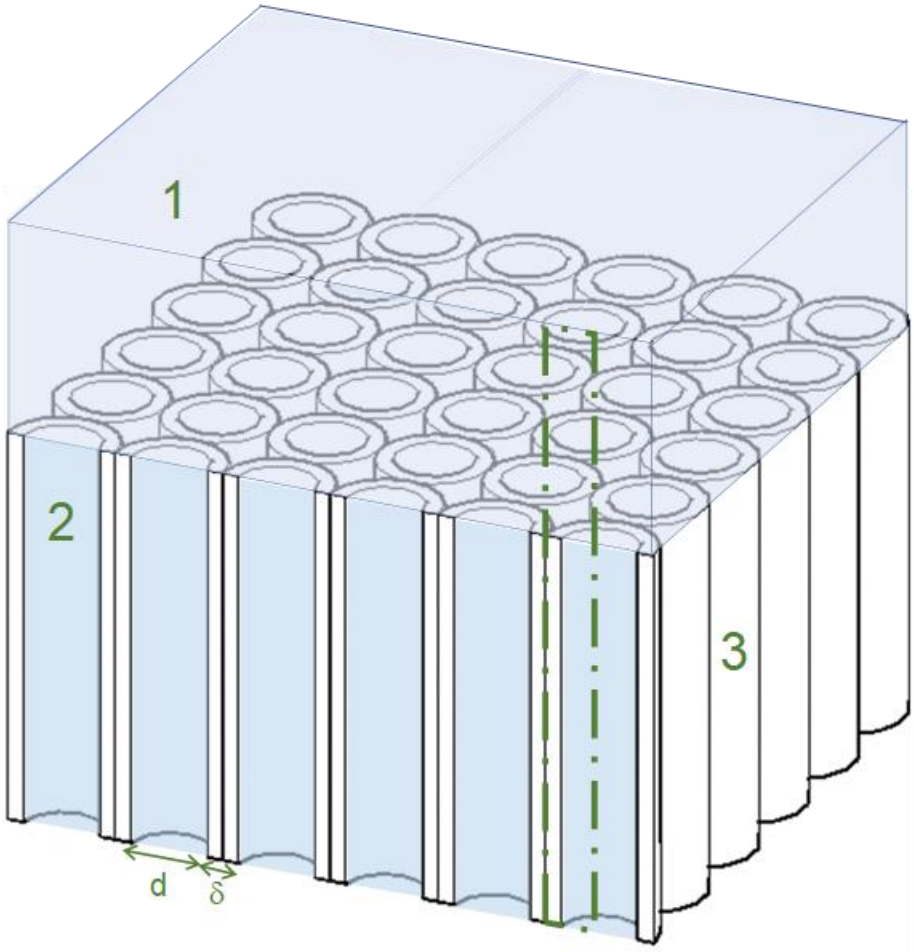

Figure 1

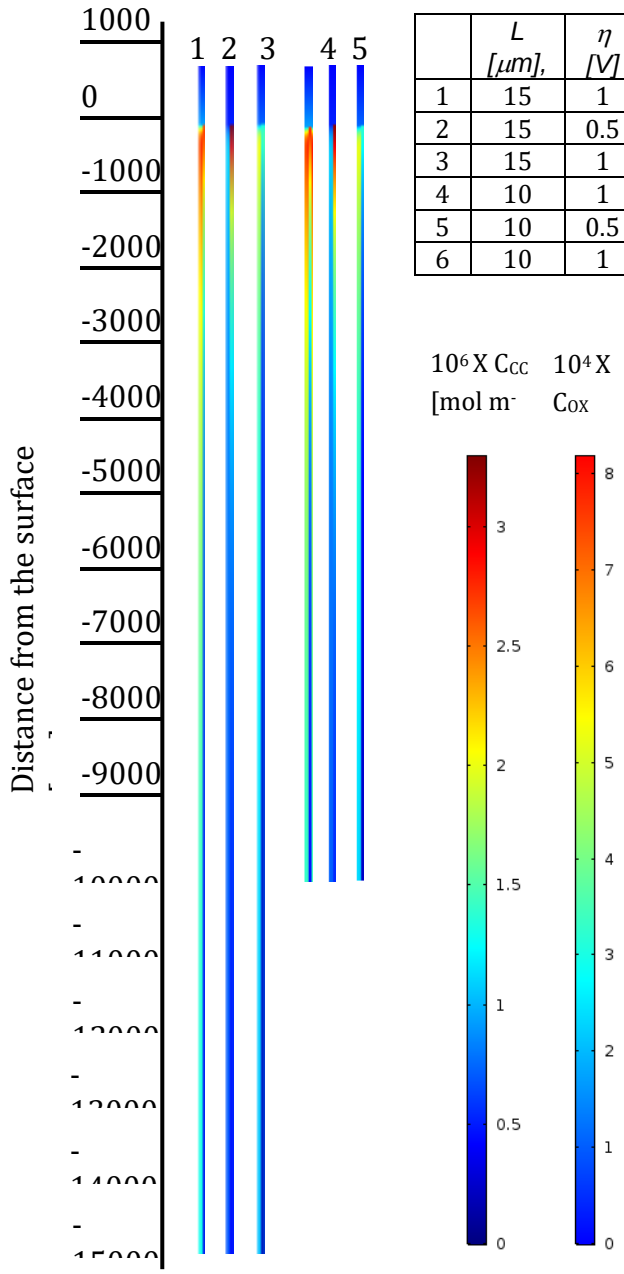

	L [*μm*],	*η* [*V*]	I_0 [*W m*$^{-2}$]
1	15	1	1000
2	15	0.5	1000
3	15	1	500
4	10	1	1000
5	10	0.5	1000
6	10	1	500

Figure 2

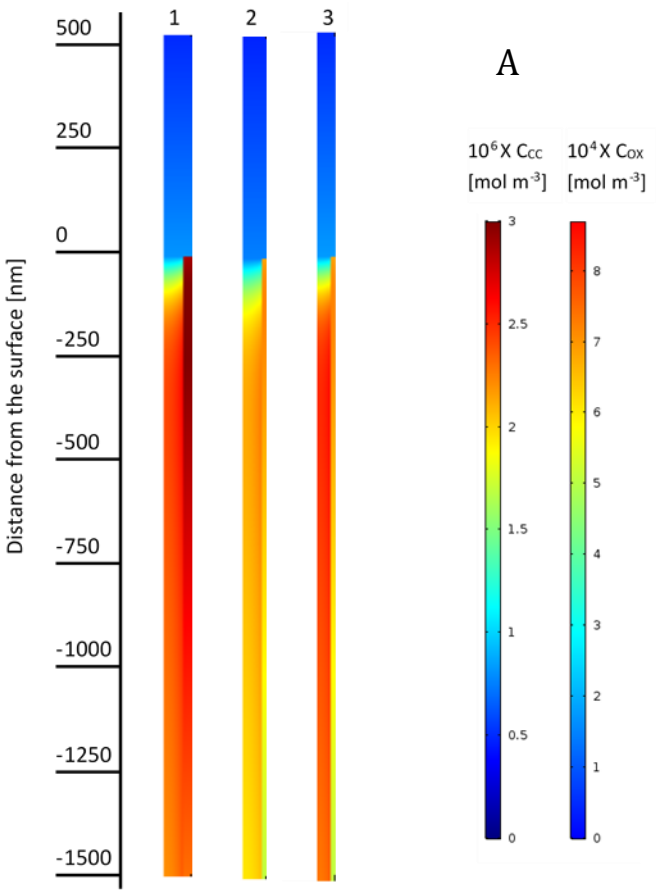
A
1
2
3
500
250
0
-250
-500
-750
-1000
-1250
-1500
Distance from the surface [nm]
10⁶X Ccc [mol m⁻³]
10⁴X Cox [mol m⁻³]
3
2.5
2
1.5
1
0.5
0
8
7
6
5
4
3
2
1
0

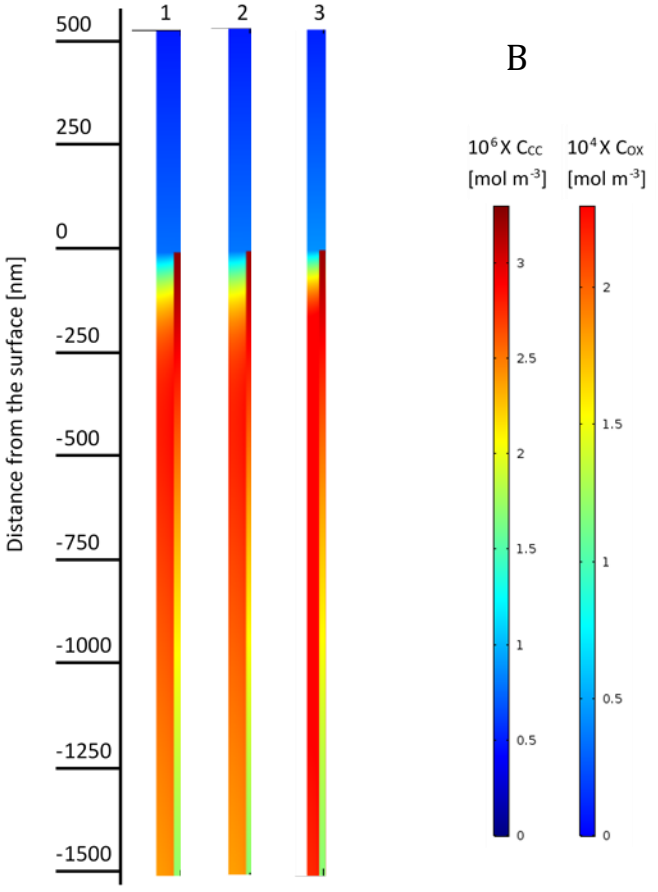
B
1
2
3
500
250
0
-250
-500
-750
-1000
-1250
-1500
Distance from the surface [nm]
10⁶X Ccc [mol m⁻³]
10⁴X Cox [mol m⁻³]
3
2.5
2
1.5
1
0.5
0
2
1.5
1
0.5
0

Figure 3

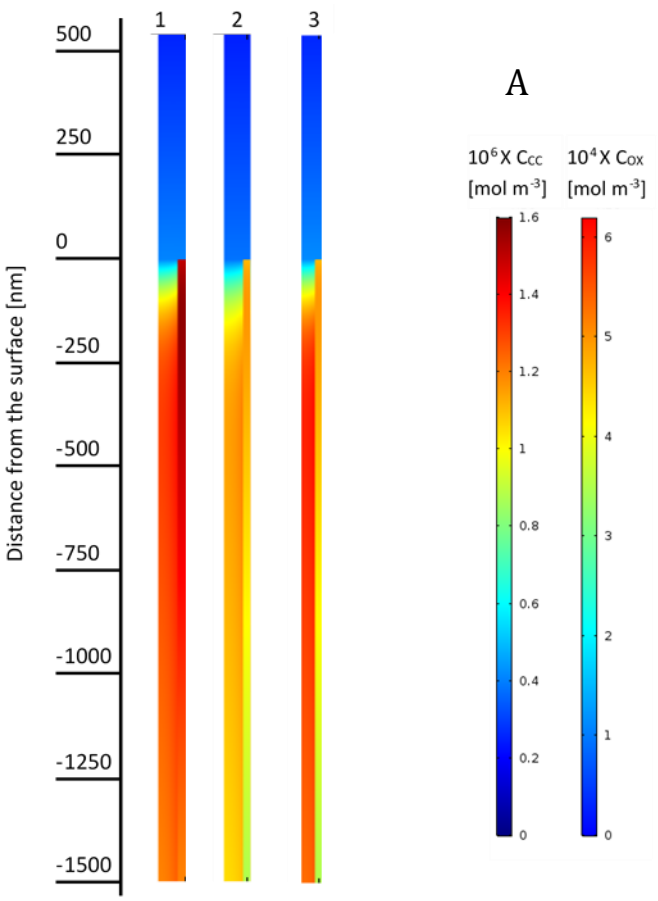
A
1
2
3
500
250
0
-250
-500
-750
-1000
-1250
-1500
Distance from the surface [nm]
10⁶X Ccc [mol m⁻³]
10⁴X Cox [mol m⁻³]
1.6
1.4
1.2
1
0.8
0.6
0.4
0.2
0
6
5
4
3
2
1
0

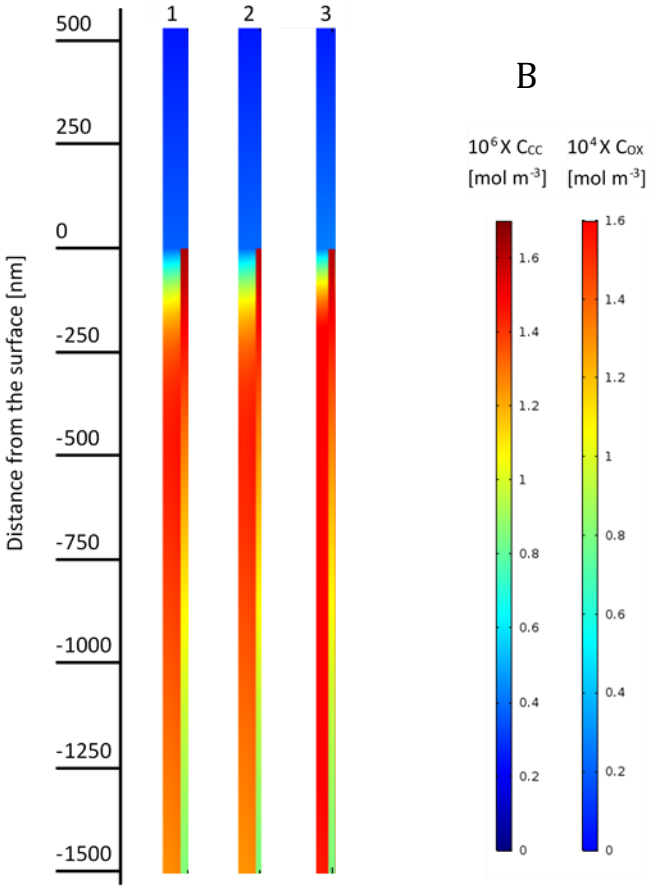
B
1
2
3
500
250
0
-250
-500
-750
-1000
-1250
-1500
Distance from the surface [nm]
10⁶X Ccc [mol m⁻³]
10⁴X Cox [mol m⁻³]
1.6
1.4
1.2
1
0.8
0.6
0.4
0.2
0

Figure 4

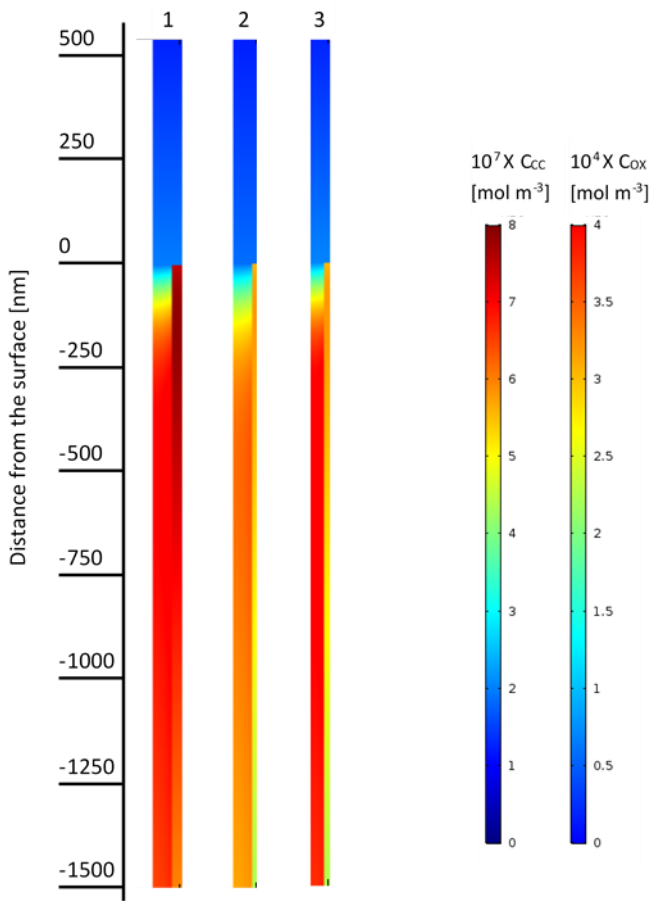
1
2
3
500
250
0
-250
-500
-750
-1000
-1250
-1500
Distance from the surface [nm]
10⁷X Ccc
[mol m⁻³]
10⁴X Cox
[mol m⁻³]
8
7
6
5
4
3
2
1
0
4
3.5
3
2.5
2
1.5
1
0.5
0

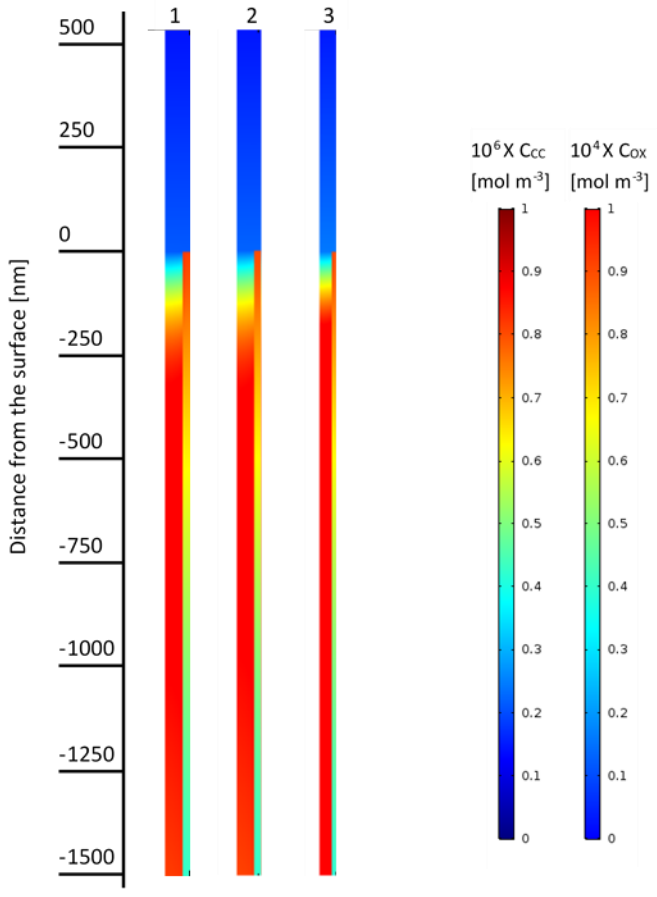
1
2
3
500
250
0
-250
-500
-750
-1000
-1250
-1500
Distance from the surface [nm]
10⁶X Ccc
[mol m⁻³]
10⁴X Cox
[mol m⁻³]
1
0.9
0.8
0.7
0.6
0.5
0.4
0.3
0.2
0.1
0

Figure 5

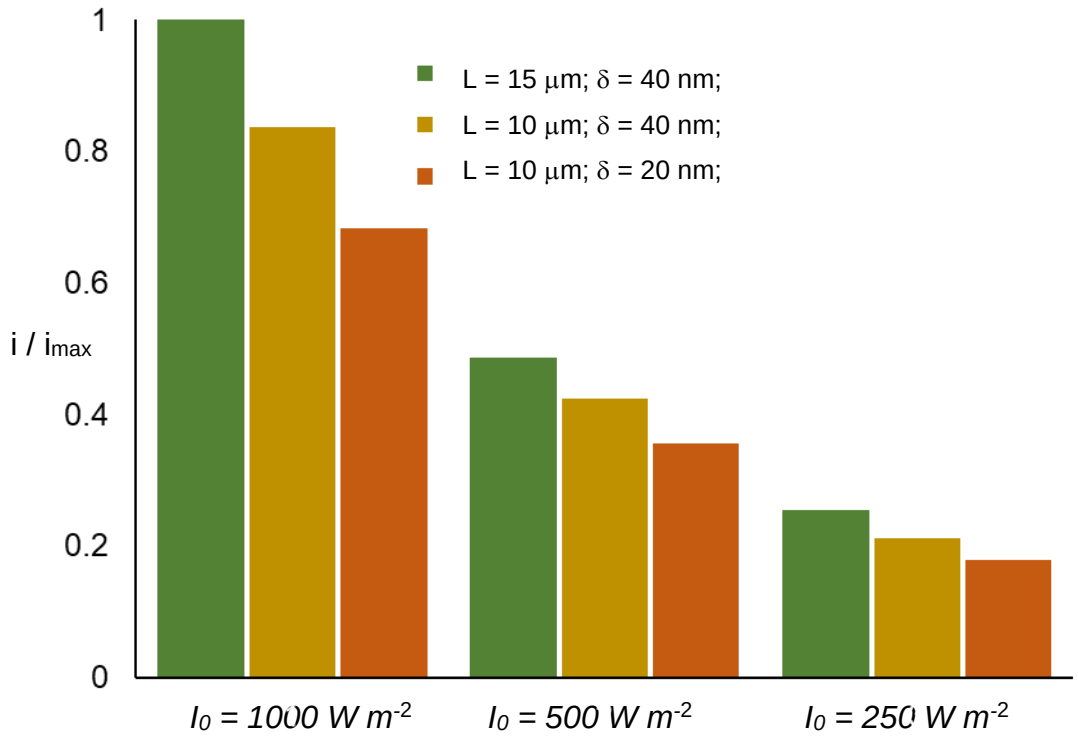
1
0.8
0.6
i / imax
0.4
0.2
0
L = 15 μm; δ = 40 nm;
L = 10 μm; δ = 40 nm;
L = 10 μm; δ = 20 nm;
I0 = 1000 W m-2
I0 = 500 W m-2
I0 = 250 W m-2

Figure 6

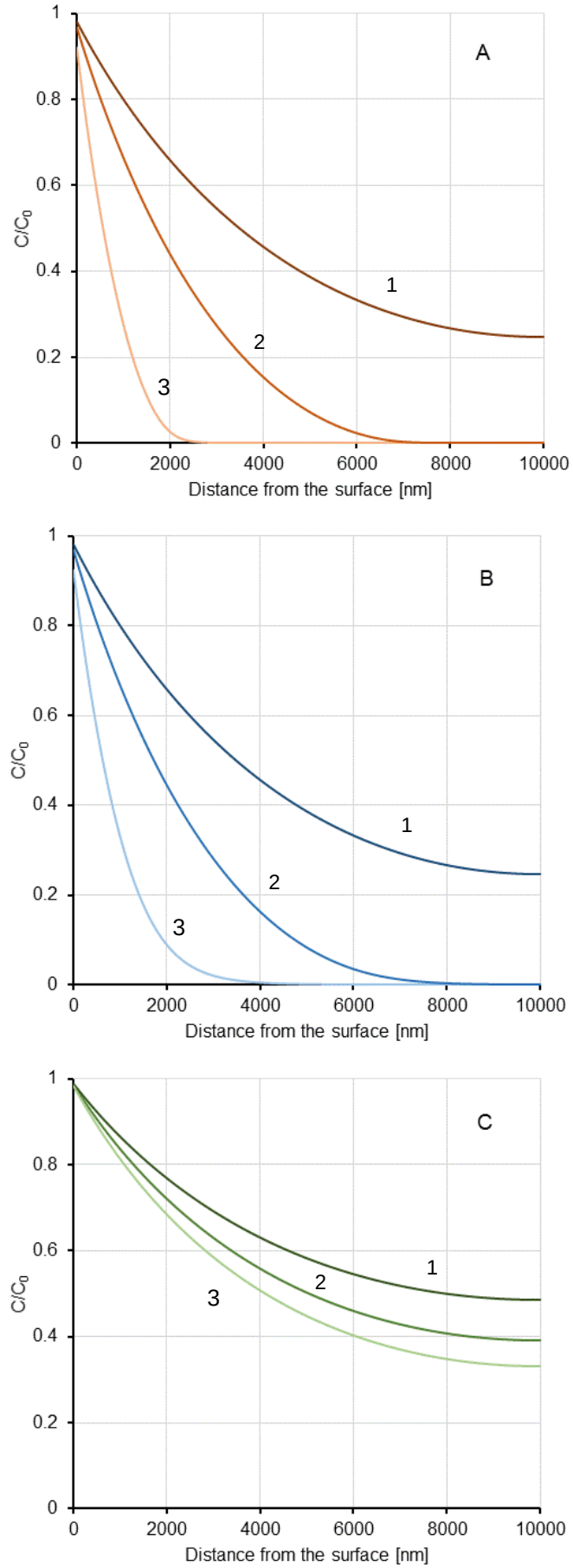
A
B
C
C/C0
Distance from the surface [nm]
0
0.2
0.4
0.6
0.8
1
2000
4000
6000
8000
10000
1
2
3

Figure 7

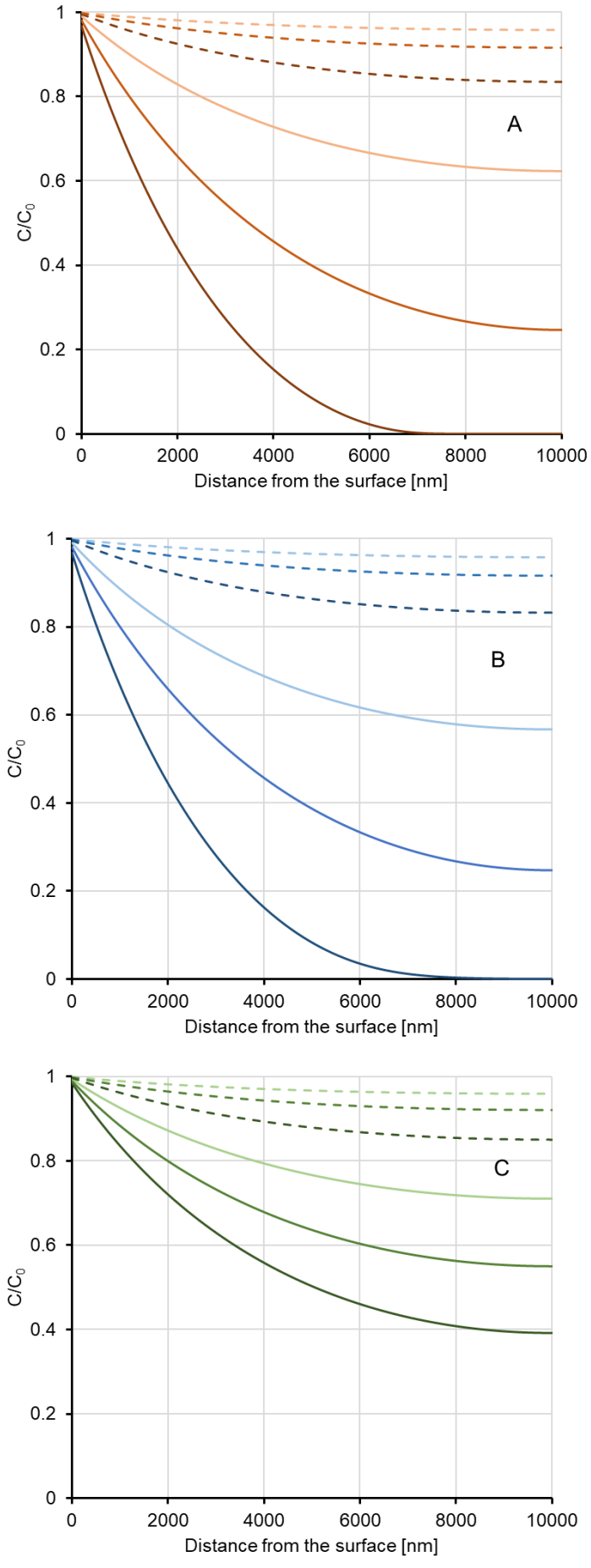
A
B
C
C/C0
Distance from the surface [nm]
0
0.2
0.4
0.6
0.8
1
0
2000
4000
6000
8000
10000

Figure 8

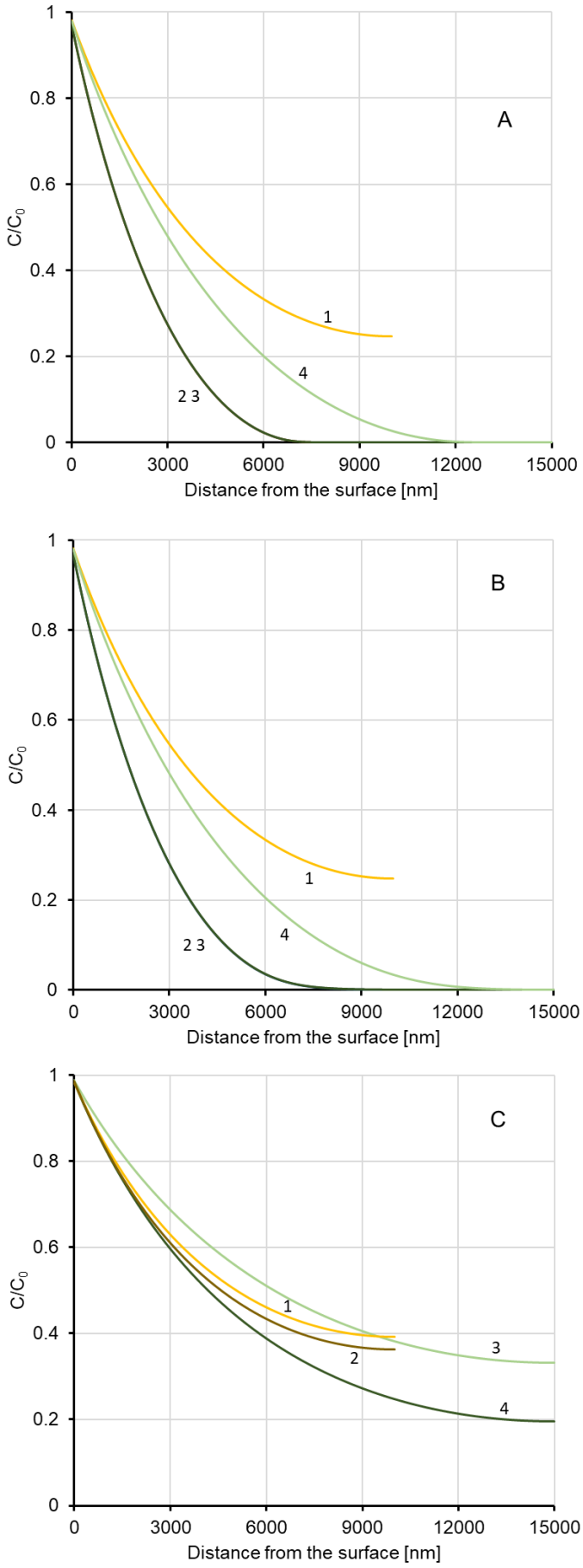
A
B
C
C/C0
Distance from the surface [nm]
0
0.2
0.4
0.6
0.8
1
3000
6000
9000
12000
15000
1
2 3
4
2
3

Figure 9

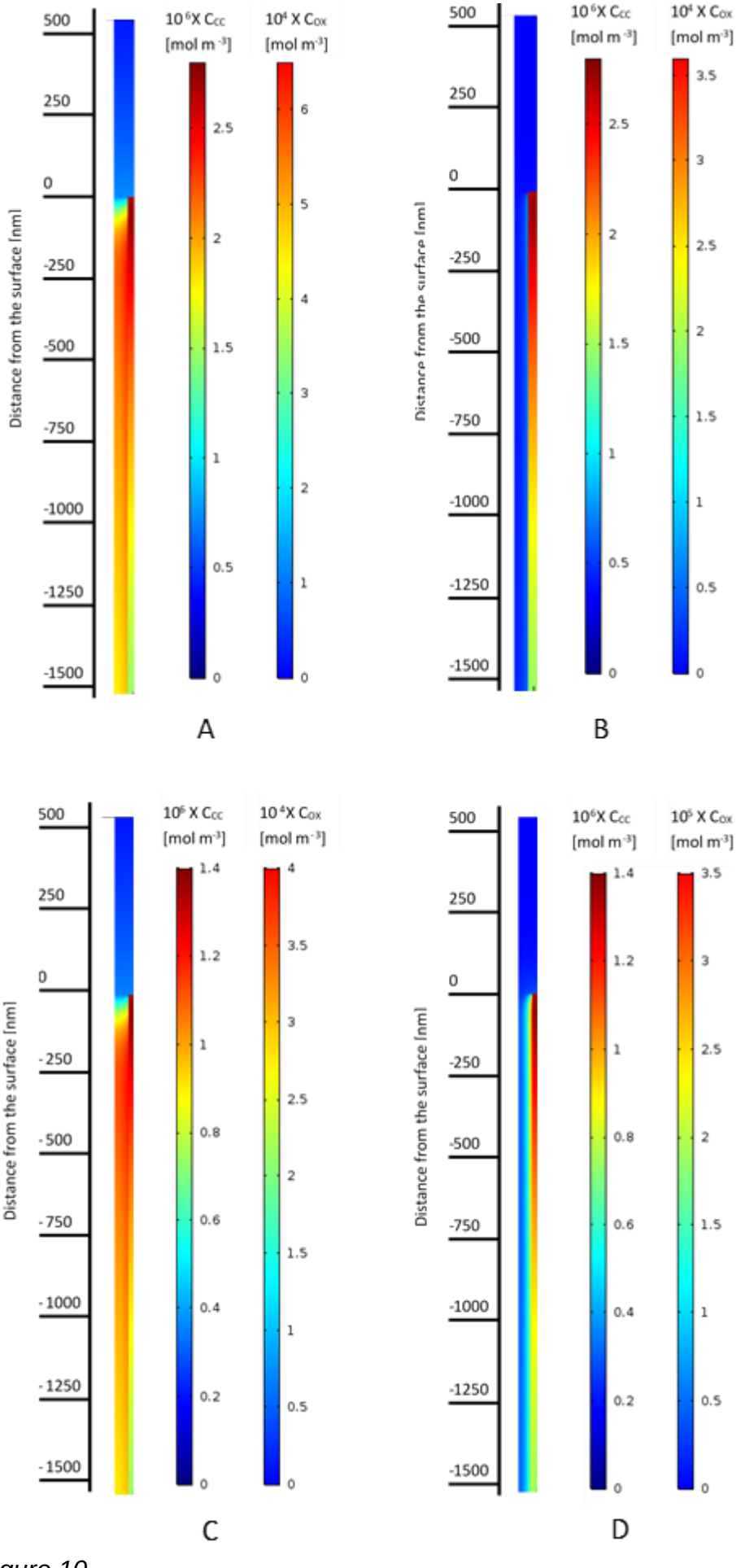
Distance from the surface [nm]
500
250
0
-250
-500
-750
-1000
-1250
-1500
10⁶X Ccc [mol m⁻³]
2.5
2
1.5
1
0.5
0
10⁴ X Cox [mol m⁻³]
6
5
4
3
2
1
0
A
10⁶X Ccc [mol m⁻³]
3.5
3
2.5
2
1.5
1
0.5
0
10⁴ X Cox [mol m⁻³]
B
10⁶ X Ccc [mol m⁻³]
1.4
1.2
1
0.8
0.6
0.4
0.2
0
10⁴X Cox [mol m⁻³]
4
3.5
3
2.5
2
1.5
1
0.5
0
C
10⁶X Ccc [mol m⁻³]
10⁵ X Cox [mol m⁻³]
D

Figure 10.

Figure captions

Figure 1: sketch of the nanotubular structure (not in scale) with domains of integration: 1) Diffusion layer, 2) Liquid phase (pores); 3) Solid phase. Dash-dotted line is the contour of the surface plots in figures 2-5 and 7-9.

Figure 2: examples of space profiles of oxygenated radicals inside the pore and in the diffusion layer, and of charge carriers in the pore wall under different conditions with d = 100 nm, and δ = 20 nm.

Figure 3: space profiles of oxygenated radicals in pore and diffusion layer, and of charge carriers in the pore wall. Data obtained with 10 μm pore length, I_0 = 1000 W m^{-2}, η = 1 V (A) and *η = 0.5 V (B) and different geometries.1: d = 100 nm, δ = 40 nm; 2: d = 100 nm, δ = 20 nm; 3: d = 70 nm, δ = 20 nm.*

Figure 4: space profiles of oxygenated radicals in pore and diffusion layer, and of charge carriers in the pore wall. Data obtained with 10 μm pore length, I_0 = 500 W m^{-2}, η = 1 V (A) and *η = 0.5 V (B) and different geometries.1: d = 100 nm, δ = 40 nm; 2: d = 100 nm, δ = 20 nm; 3: d = 70 nm, δ = 20 nm.*

Figure 5: space profiles of oxygenated radicals in pore and diffusion layer, and of charge carriers in the pore wall. Data obtained with 10 μm pore length, I_0 = 250 W m^{-2}, η = 1 V (A) and *η = 0.5 V (B) and different geometries.1: d = 100 nm, δ = 40 nm; 2: d = 100 nm, δ = 20 nm; 3: d = 70 nm, δ = 20 nm.*

Figure 6: Current intensities, normalised with the maximum value, calculated with d = 100 nm and η = 1V.

Figure 7. Space profiles of Phenol (A), Paraquat (B) and Oxalic Acid (C) along the pore axis. Data calculated with pore length of 10 μm, δ = 40 nm, d = 100 nm, η = 1 V, I_0 = 1000 W m^{-2} and different bulk concentrations (C_0). 1: C_0= 1 mol m^{-3}; 2: C_0= 0.5 mol m^{-3}; 3: C_0= 0.1 mol m^{-3}.

Figure 8. Space profiles of Phenol (A), Paraquat (B) and Oxalic Acid (C) along the pore axis. Data calculated with pore length of 10 μm, δ = 40 nm, d = 100 nm, C_0= 0.5 mol m^{-3}, η = 1 V (full lines) and η = 0.5 V (dashed lines) and different light intensities. 1: I_0 = 1000 W m^{-2}; 2: I_0 = 500 W m^{-2}; 3: I_0 = 250 W m^{-2}

Figure 9. Space profiles of Phenol (A), Paraquat (B) and Oxalic Acid (C) along the pore axis. Data calculated with C_0= 0.5 mol m^{-3}, d = 100 nm, η = 1 V and different pore geometries and light intensities. 1: pore length 10 μm, δ = 20 nm, I_0 = 1000 W m^{-2}; 2: pore length 10 μm, δ = 40 nm, I_0 = 1000 W m^{-2}; 3: pore length 15 μm, δ = 20 nm, I_0 = 1000 W m^{-2}; 4: pore length 15 μm, δ = 20 nm, I_0 = 500 W m^{-2}

Figure 10: space profiles of oxygenated radicals in pore and diffusion layer, and of charge carriers in the pore wall. Data obtained with L = 10 μm, δ = 20 nm, d = 100 nm, η = 1 V,

with C_0= 0.5 mol m^{-3} of Paraquat or Oxalic acid. *A: Paraquat*, I_0 = *1000 W* m^{-2}; B*: Paraquat*, I_0 = *500 W* m^{-2}; *C: Oxalic Acid*, I_0 = *1000 W* m^{-2}; *D: Oxalic Acid*, I_0 = *500W* m^{-2}*.*